

INCOMMENSURATE SPIN DYNAMICS IN UNDERDOPED CUPRATE PEROVSKITES

A. Sherman

Institute of Physics, University of Tartu, Riia 142, 51014 Tartu, Estonia
alexei@fi.tartu.ee

M. Schreiber

Institut für Physik, Technische Universität, D-09107 Chemnitz, Federal Republic of Germany

Received Day Month Year

Revised Day Month Year

The incommensurate magnetic response observed in normal-state cuprate perovskites is interpreted based on the projection operator formalism and the t - J model of Cu-O planes. In agreement with experiment the calculated dispersion of maxima in the susceptibility has the shape of two parabolas with upward and downward branches which converge at the antiferromagnetic wave vector. The maxima are located at the momenta $(\frac{1}{2}, \frac{1}{2} \pm \delta)$, $(\frac{1}{2} \pm \delta, \frac{1}{2})$ and at $(\frac{1}{2} \pm \delta, \frac{1}{2} \pm \delta)$, $(\frac{1}{2} \pm \delta, \frac{1}{2} \mp \delta)$ in the lower and upper parabolas, respectively. The upper parabola reflects the dispersion of magnetic excitations of the localized Cu spins, while the lower parabola arises due to a dip in the spin-excitation damping at the antiferromagnetic wave vector. For moderate doping this dip stems from the weakness of the interaction between the spin excitations and holes near the hot spots. The frequency dependence of the susceptibility is shown to depend strongly on the hole bandwidth and damping and varies from the shape observed in $\text{YBa}_2\text{Cu}_3\text{O}_{7-y}$ to that inherent in $\text{La}_{2-x}\text{Sr}_x\text{CuO}_4$.

Keywords: Cuprate superconductors; magnetic properties; t - J model.

1. Introduction

One of the most interesting features of the inelastic neutron scattering in lanthanum cuprates is that for hole concentrations $x \gtrsim 0.04$, low temperatures and small energy transfers the scattering is peaked at incommensurate momenta $(\frac{1}{2}, \frac{1}{2} \pm \delta)$, $(\frac{1}{2} \pm \delta, \frac{1}{2})$ in the reciprocal lattice units $2\pi/a$ with the lattice period a .¹ For $x \lesssim 0.12$ the incommensurability parameter δ is approximately equal to x .² For larger x the parameter saturates near the value $\delta \approx 0.12$. The incommensurate response was observed both below and above T_c .³ Recently the analogous low-frequency incommensurability was observed also in $\text{YBa}_2\text{Cu}_3\text{O}_{7-y}$.⁴ This gives ground to suppose that the incommensurability is a common feature of cuprate perovskites which does not depend on subtle details of the energy structure. However, for larger frequencies the susceptibility differs essentially in these two types of cuprates. In the underdoped $\text{YBa}_2\text{Cu}_3\text{O}_{7-y}$ and some other cuprates both below and above T_c a pronounced maximum is ob-

served at frequencies $\omega_r = 25 - 40$ meV.⁵ In the momentum space the magnetic response is sharply peaked at the antiferromagnetic wave vector $\mathbf{Q} = (\frac{1}{2}, \frac{1}{2})$ for this frequency. Contrastingly, no maximum at ω_r was observed in lanthanum cuprates. Instead for low temperatures and frequencies of several millielectronvolts a broad feature was detected.⁶ For even larger frequencies the magnetic response becomes again incommensurate in both types of cuprates with peaks located at $(\frac{1}{2} \pm \delta, \frac{1}{2} \pm \delta)$, $(\frac{1}{2} \pm \delta, \frac{1}{2} \mp \delta)$.^{5,7,8,9} In contrast to the low-frequency incommensurability in which the incommensurability parameter decreases with increasing frequency, the parameter of the high-frequency incommensurability grows or remains practically unchanged with frequency. Thus, the dispersion of maxima in the susceptibility resembles two parabolas with upward- and downward-directed branches which converge at \mathbf{Q} and near the frequency ω_r .^{4,9}

The nature of the magnetic incommensurability is the subject of active discussion now. The most frequently used approaches for its explanation are based on the picture of itinerant electrons with the susceptibility calculated in the random phase approximation^{10,11} and on the stripe domain picture.^{9,12} In the former approach the low-frequency incommensurability is connected with the Fermi surface nesting in the normal state or with the nesting in constant-energy contours in the superconducting case. This imposes rather stringent requirements on the electron energy spectrum, since the nesting has to persist in the range of hole concentrations $0.04 \lesssim x \lesssim 0.18$ where the incommensurability is observed and the nesting momentum has to change in a specific manner with doping to ensure the known dependence of the incommensurability parameter δ on x . It is unlikely that these conditions are fulfilled in $\text{La}_{2-x}\text{Sr}_x\text{CuO}_4$.¹³ Besides, the applicability of the picture of itinerant electrons for underdoped cuprates casts doubts. As for the second notion, it should be noted that in the elastic neutron scattering the charge-density wave connected with stripes is observed only in crystals with the low-temperature tetragonal or the low-temperature less-orthorhombic phases ($\text{La}_{2-x}\text{Ba}_x\text{CuO}_4$ and $\text{La}_{2-y-x}\text{Nd}_y\text{Sr}_x\text{CuO}_4$) and is not observed in the crystal $\text{La}_{2-x}\text{Sr}_x\text{CuO}_4$ in the low-temperature orthorhombic phase.¹⁴ At the same time the magnetic incommensurability is similar in these phases. It can be supposed that the magnetic incommensurability is the cause rather than the effect of stripes which are formed with an assistance of phonons.

In the present work the general formula for the magnetic susceptibility derived in the projection operator formalism¹⁵ is used. For the description of spin excitations in the doped antiferromagnet the t - J model of a Cu-O plane is employed. In this approach the mentioned peculiarities of the magnetic properties of cuprates are reproduced including the proper frequency and momentum location of the susceptibility maxima. The incommensurability for $\omega > \omega_r$ is connected with the dispersion of spin excitations.^{16,17} The incommensurability for lower frequencies is related to the dip in the spin-excitation damping at \mathbf{Q} . For small x the dip appears due to the nesting of the hole pockets around $(\pm\frac{1}{4}, \pm\frac{1}{4})$ forming the Fermi surface.¹⁸ For

moderate doping this dip stems from the weakness of the interaction between the spin excitations and holes near the hot spots – the intersection points of the Fermi surface and the boundary of the magnetic Brillouin zone. Such a weak interaction follows from the fact that due to a short-range interaction between holes and spins a decaying site spin excitation creates a fermion pair with components residing on the same and neighbor sites. The spin-excitation damping was found to depend strongly on details of the hole dispersion, bandwidth and damping, so that the change in these characteristics leads to the conversion of well-defined spin excitations to overdamped ones. As this takes place, the frequency dependence of the susceptibility at \mathbf{Q} is transformed from a pronounced maximum⁵ at ω_r which is inherent in underdoped $\text{YBa}_2\text{Cu}_3\text{O}_{7-y}$ to a broad low-frequency feature characteristic for lanthanum cuprates.⁶ The increased spin-excitation damping has no marked effect on the low-frequency incommensurability, however for $\omega > \omega_r$ the incommensurate peaks are shifted to \mathbf{Q} and form a broad maximum. Such form of the momentum dependence of the susceptibility is also observed experimentally.¹⁹

2. Main formulas

The imaginary part of the magnetic susceptibility which determines the cross-section of the magnetic scattering²⁰ is calculated from the relations $\chi''(\mathbf{k}\omega) = -4\mu_B^2 \Im \langle \langle s_{\mathbf{k}}^z | s_{-\mathbf{k}}^z \rangle \rangle_\omega$, $\langle \langle s_{\mathbf{k}}^z | s_{-\mathbf{k}}^z \rangle \rangle_\omega = \omega((s_{\mathbf{k}}^z | s_{-\mathbf{k}}^z))_\omega - (s_{\mathbf{k}}^z, s_{-\mathbf{k}}^z)$. Here μ_B is the Bohr magneton, $\langle \langle s_{\mathbf{k}}^z | s_{-\mathbf{k}}^z \rangle \rangle_\omega$ and $((s_{\mathbf{k}}^z | s_{-\mathbf{k}}^z))_\omega$ are the Fourier transforms of the retarded Green's and Kubo's relaxation functions,

$$\langle \langle s_{\mathbf{k}}^z | s_{-\mathbf{k}}^z \rangle \rangle_t = -i\theta(t) \langle [s_{\mathbf{k}}^z(t), s_{-\mathbf{k}}^z] \rangle, \quad ((s_{\mathbf{k}}^z | s_{-\mathbf{k}}^z))_t = \theta(t) \int_t^\infty dt' \langle [s_{\mathbf{k}}^z(t'), s_{-\mathbf{k}}^z] \rangle,$$

$s_{\mathbf{k}}^z = N^{-1/2} \sum_{\mathbf{n}} e^{-i\mathbf{k}\mathbf{n}} s_{\mathbf{n}}^z$ with the number of sites N and the z component of the spin $s_{\mathbf{n}}^z$ on the lattice site \mathbf{n} , for arbitrary operators A and B $(A, B) = i \int_0^\infty dt \langle [A(t), B] \rangle$ where the angular brackets denote the statistical averaging and $A(t) = e^{iHt} A e^{-iHt}$ with the Hamiltonian H .

Using the projection operator technique¹⁵ the relaxation function $((s_{\mathbf{k}}^z | s_{-\mathbf{k}}^z))_\omega$ can be calculated from the recursive relations

$$R_n(\omega) = [\omega - E_n - F_n R_{n+1}(\omega)]^{-1}, \quad n = 0, 1, 2, \dots \quad (1)$$

where $R_n(\omega)$ is the Laplace transform of $R_n(t) = (A_{nt}, A_n^\dagger)(A_n, A_n^\dagger)^{-1}$, the time dependence in A_{nt} is determined by the relation

$$i \frac{d}{dt} A_{nt} = \prod_{k=0}^{n-1} (1 - P_k) [A_{nt}, H], \quad A_{n,t=0} = A_n$$

with the projection operators P_k defined as $P_k B = (B, A_k^\dagger)(A_k, A_k^\dagger)^{-1} A_k$. The parameters E_n and F_n in relations (1) and operators A_n in the functions $R_n(t)$ are calculated recursively using the procedure¹⁷

$$[A_n, H] = E_n A_n + A_{n+1} + F_{n-1} A_{n-1}, \quad E_n = ([A_n, H], A_n^\dagger)(A_n, A_n^\dagger)^{-1},$$

(2)

$$F_{n-1} = (A_n, A_n^\dagger)(A_{n-1}, A_{n-1}^\dagger)^{-1}, \quad F_{-1} = 0.$$

As the starting operator for this procedure we set $A_0 = s_{\mathbf{k}}^z$. In this case $((s_{\mathbf{k}}^z | s_{-\mathbf{k}}^z))_\omega = (s_{\mathbf{k}}^z, s_{-\mathbf{k}}^z) R_0(\omega)$ where $R_0(\omega)$ is calculated from Eq. (1).

To describe the spin excitations of Cu-O planes which determine the magnetic properties of cuprates²⁰ the t - J model²¹ is used. The model was shown to describe correctly the low-energy part of the spectrum of the realistic extended Hubbard model.^{22,23} The Hamiltonian of the two-dimensional t - J model reads

$$H = \sum_{\mathbf{n}\mathbf{m}\sigma} t_{\mathbf{n}\mathbf{m}} a_{\mathbf{n}\sigma}^\dagger a_{\mathbf{m}\sigma} + \frac{1}{2} \sum_{\mathbf{n}\mathbf{m}} J_{\mathbf{n}\mathbf{m}} s_{\mathbf{n}} s_{\mathbf{m}}, \quad (3)$$

where $a_{\mathbf{n}\sigma} = |\mathbf{n}\sigma\rangle\langle\mathbf{n}0|$ is the hole annihilation operator, \mathbf{n} and \mathbf{m} label sites of the square lattice, $\sigma = \pm 1$ is the spin projection, $J_{\mathbf{n}\mathbf{m}}$ and $t_{\mathbf{n}\mathbf{m}}$ are the exchange and hopping constants, respectively, $|\mathbf{n}\sigma\rangle$ and $|\mathbf{n}0\rangle$ are site states corresponding to the absence and presence of a hole on the site. These states may be considered as linear combinations of the products of the $3d_{x^2-y^2}$ copper and $2p_\sigma$ oxygen orbitals of the extended Hubbard model.²³ The spin- $\frac{1}{2}$ operators can be written as $s_{\mathbf{n}}^z = \frac{1}{2} \sum_{\sigma} \sigma |\mathbf{n}\sigma\rangle\langle\mathbf{n}\sigma|$ and $s_{\mathbf{n}}^\sigma = |\mathbf{n}\sigma\rangle\langle\mathbf{n}, -\sigma|$.

With Hamiltonian (3) and $A_0 = s_{\mathbf{k}}^z$ we find from Eq. (2)

$$\begin{aligned} E_0(s_{\mathbf{k}}^z, s_{-\mathbf{k}}^z) &= (i\dot{s}_{\mathbf{k}}^z, s_{-\mathbf{k}}^z) = \langle [s_{\mathbf{k}}^z, s_{-\mathbf{k}}^z] \rangle = 0, \\ A_1 &= A_1^s + A_1^h = \frac{1}{2\sqrt{N}} \sum_{\mathbf{l}} e^{-i\mathbf{k}\mathbf{l}} \left[\sum_{\mathbf{n}\mathbf{m}} J_{\mathbf{m}\mathbf{n}} (\delta_{\mathbf{l}\mathbf{n}} - \delta_{\mathbf{l}\mathbf{m}}) s_{\mathbf{n}}^{+1} s_{\mathbf{m}}^{-1} \right. \\ &\quad \left. + \sum_{\mathbf{n}\mathbf{m}\sigma} t_{\mathbf{m}\mathbf{n}} (\delta_{\mathbf{l}\mathbf{m}} - \delta_{\mathbf{l}\mathbf{n}}) \sigma a_{\mathbf{n}\sigma}^\dagger a_{\mathbf{m}\sigma} \right], \end{aligned} \quad (4)$$

where $i\dot{s}_{\mathbf{k}}^z = [s_{\mathbf{k}}^z, H]$. To obtain a tractable form for the spin-excitation damping it is convenient to approximate the quantity (A_{1t}, A_1^\dagger) in the $R_1(\omega)$ by the sum

$$(A_1^h(t), A_1^{h\dagger}) + (A_{1t}^s, A_1^{s\dagger})$$

where the first term describes the influence of holes on the spin excitations. Continuing calculations (2) with the second term of the sum we get

$$F_0 = 4JC_1(\gamma_{\mathbf{k}} - 1)(s_{\mathbf{k}}^z, s_{-\mathbf{k}}^z)^{-1}, \quad E_1 = 0, \quad (5)$$

where only the nearest neighbor interaction between spins was taken into account, $J_{\mathbf{n}\mathbf{m}} = J \sum_{\mathbf{a}} \delta_{\mathbf{n}, \mathbf{m}+\mathbf{a}}$, the four vectors \mathbf{a} connect the nearest neighbor sites, $C_1 = \langle s_{\mathbf{n}}^{+1} s_{\mathbf{n}+\mathbf{a}}^{-1} \rangle$ is the spin correlation on neighbor sites and $\gamma_{\mathbf{k}} = \frac{1}{2} [\cos(k_x) + \cos(k_y)]$.

To calculate the quantity $(s_{\mathbf{k}}^z, s_{-\mathbf{k}}^z)$ let us notice that in accord with procedure (2) the interruption of calculations at this stage actually means that (A_2, A_2^\dagger) in the parameter F_1 is set to zero. Here $A_2 = i^2 \ddot{s}_{\mathbf{k}}^z - F_0 s_{\mathbf{k}}^z$. The substitution of this expression into $(A_2, A_2^\dagger) = 0$ gives an equation for $(s_{\mathbf{k}}^z, s_{-\mathbf{k}}^z)$. Using the decoupling in calculating $i^2 \ddot{s}_{\mathbf{k}}^z$ we get¹⁷

$$(s_{\mathbf{k}}^z, s_{-\mathbf{k}}^z)^{-1} = 4\alpha J(\Delta + 1 + \gamma_{\mathbf{k}}), \quad (6)$$

where $\alpha \sim 1$ is the decoupling parameter.²⁴ The meaning of the parameter Δ , which can be expressed in terms of spin correlations, will be discussed later.

Using the decoupling in $(A_1^h(t), A_1^{h\dagger})$ we find from the above formulas

$$\chi''(\mathbf{k}\omega) = -\frac{4\mu_B^2\omega\Im R(\mathbf{k}\omega)}{[\omega^2 - \omega f_{\mathbf{k}}\Re R(\mathbf{k}\omega) - \omega_{\mathbf{k}}^2]^2 + [\omega f_{\mathbf{k}}\Im R(\mathbf{k}\omega)]^2}, \quad (7)$$

where

$$\begin{aligned} f_{\mathbf{k}}^{-1} &= 4J|C_1|(1 - \gamma_{\mathbf{k}}), \quad \omega_{\mathbf{k}}^2 = 16J^2\alpha|C_1|(1 - \gamma_{\mathbf{k}})(\Delta + 1 + \gamma_{\mathbf{k}}), \\ \Im R(\mathbf{k}\omega) &= \frac{8\pi\omega_{\mathbf{k}}^2}{N} \sum_{\mathbf{k}'} g_{\mathbf{k}\mathbf{k}'}^2 \int_{-\infty}^{\infty} d\omega' A(\mathbf{k}'\omega') \\ &\quad \times A(\mathbf{k} + \mathbf{k}', \omega + \omega') \frac{n_F(\omega + \omega') - n_F(\omega')}{\omega}, \end{aligned} \quad (8)$$

the interaction constant $g_{\mathbf{k}\mathbf{k}'} = t_{\mathbf{k}'} - t_{\mathbf{k}+\mathbf{k}'}$ with $t_{\mathbf{k}} = \sum_{\mathbf{n}} e^{i\mathbf{k}(\mathbf{n}-\mathbf{m})} t_{\mathbf{n}\mathbf{m}}$, $n_F(\omega) = [\exp(\omega/T) + 1]^{-1}$, T is the temperature and $A(\mathbf{k}\omega)$ is the hole spectral function. Since the incoherent part of the spectral function is unlikely to lead to sharp structure in χ'' , only the coherent part of $A(\mathbf{k}\omega)$ is taken into account in this work,

$$A(\mathbf{k}\omega) = \frac{\eta/\pi}{(\omega - \varepsilon_{\mathbf{k}} + \mu)^2 + \eta^2}. \quad (9)$$

Here μ is the chemical potential, η is the artificial broadening, and $\varepsilon_{\mathbf{k}}$ is the hole dispersion. The real part of $R(\mathbf{k}\omega)$ can be calculated from the imaginary part $\Im R(\mathbf{k}\omega)$ and the Kramers-Kronig relation.

Notice that the interaction constant $g_{\mathbf{k}\mathbf{k}'}$ is determined by the Fourier transform of the hole hopping constant $t_{\mathbf{n}\mathbf{m}}$. If the hopping to the nearest and next nearest sites is taken into account the constant acquires the form

$$g_{\mathbf{k}\mathbf{k}'} = t(\gamma_{\mathbf{k}'} - \gamma_{\mathbf{k}+\mathbf{k}'}) + t'(\gamma'_{\mathbf{k}'} - \gamma'_{\mathbf{k}+\mathbf{k}'}), \quad (10)$$

where $\gamma'_{\mathbf{k}} = \cos(k_x)\cos(k_y)$. This constant vanishes for $\mathbf{k} = \mathbf{Q}$ when the vector \mathbf{k}' is located at the boundary of the magnetic Brillouin zone. In other words, fermions near hot spots interact weakly with spin excitations. This is connected with the short-range character of the interaction described by constant (10) – the decaying spin excitation on the site \mathbf{n} creates the fermion pair on the same and neighbor sites which is reflected in the above form of the interaction constant.

As the quantity $\omega f_{\mathbf{k}}\Re R(\mathbf{k}\omega)$ influences the frequency of spin excitations only near \mathbf{Q} , it is convenient to incorporate it in $\omega_{\mathbf{k}}$. This modifies the parameter $\Delta > 0$ which, as seen from Eqs. (7) and (8), describes a gap in the spin-excitation spectrum at the antiferromagnetic wave vector \mathbf{Q} . The most exact way to determine this parameter is to use the constraint of zero site magnetization

$$\langle s_{\mathbf{n}}^z \rangle = \frac{1}{2}(1 - x) - \langle s_{\mathbf{n}}^{-1} s_{\mathbf{n}}^{+1} \rangle = 0, \quad (11)$$

which has to be fulfilled in the short-range antiferromagnetic ordering. It can be shown that $\Delta \propto \xi^{-2}$ where ξ is the correlation length of the short-range order.²⁵

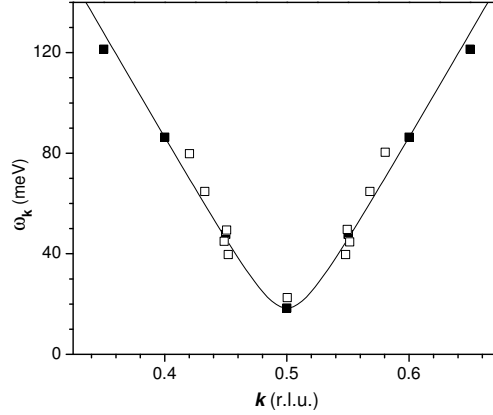


Fig. 1. The dispersion of spin excitations calculated in a 20×20 lattice for $x = 0.06$ and $T = 17$ K (filled squares).¹⁷ The solid line is the fit of Eq. (12) to these data. Open squares are the dispersion of the peak in the odd susceptibility in $\text{YBa}_2\text{Cu}_3\text{O}_{6.5}$ ($x \approx 0.075$, Ref. 26) at $T = 5$ K.⁵

Thus, in this case the frequency of spin excitations at \mathbf{Q} is nonzero, in contrast to the classical antiferromagnetic magnons. As follows from Eq. (8), the dispersion of spin excitations has a local minimum at \mathbf{Q} and can be approximated as

$$\omega_{\mathbf{k}} = [\omega_{\mathbf{Q}}^2 + c^2(\mathbf{k} - \mathbf{Q})^2]^{1/2} \quad (12)$$

near this momentum. In Fig. 1 the calculated dispersion of spin excitations¹⁷ near \mathbf{Q} is compared with the dispersion of the maximum in the susceptibility in $\text{YBa}_2\text{Cu}_3\text{O}_{6.5}$.⁵ This is a bilayer crystal and the symmetry allows one to divide the susceptibility into odd and even parts. For the antiferromagnetic intralayer coupling the dispersion of the maximum in the odd part can be compared with our calculations carried out for a single layer. This comparison demonstrates that the observed dispersion of the susceptibility maxima above $\omega_{\mathbf{Q}}$, which we identify with the resonance frequency ω_r , is closely related to the dispersion of spin excitations.

Previous calculations²⁵ show that the variation of the temperature in the range from 0 to approximately 100 K leads only to some broadening of maxima in the susceptibility. Therefore to simplify calculations and use larger lattices, which is necessary to resolve the low-frequency incommensurability, let us set $T = 0$. In calculating $\Im R(\mathbf{k}\omega)$ the integration over frequencies in Eq. (8) is the most time-consuming operation. For $T = 0$ and $\omega \geq 0$ this integral reduces to

$$\int_{-\omega}^0 d\omega' A(\mathbf{k}'\omega') A(\mathbf{k} + \mathbf{k}', \omega + \omega')$$

and is easily integrated for the spectral function (9). The same result is obtained for $\omega < 0$, since $\Im R(\mathbf{k}\omega)$ is an even function of frequency. Notice that for $\eta \ll \omega$ the states with energies

$$-\omega < \varepsilon_{\mathbf{k}'} - \mu < 0 \text{ and } 0 < \varepsilon_{\mathbf{k}+\mathbf{k}'} - \mu < \omega \quad (13)$$

make the main contribution to this integral.

In the following, we use the values of C_1 , Δ and α calculated self-consistently in the t - J model on a 20×20 lattice for the range of hole concentrations $0 \leq x \lesssim 0.16$.²⁵ The calculations were carried out for the parameters $t = 0.5$ eV and $J = 0.1$ eV corresponding to hole-doped cuprates.²⁷ In Eq. (9), for $\varepsilon_{\mathbf{k}}$ we apply the hole dispersion

$$\begin{aligned} \varepsilon_{\mathbf{k}} = & -0.0879 + 0.5547\gamma_{\mathbf{k}} - 0.1327\gamma'_{\mathbf{k}} - 0.0132\gamma_{2\mathbf{k}} \\ & + 0.09245[\cos(2k_x)\cos(k_y) + \cos(k_x)\cos(2k_y)] - 0.0265\gamma'_{2\mathbf{k}} \end{aligned} \quad (14)$$

proposed from the analysis of photoemission data in $\text{Bi}_2\text{Sr}_2\text{CaCu}_2\text{O}_8$.²⁸ Here the coefficients are in electronvolts. Results which are analogous to those discussed in the next section can also be obtained with other model dispersions suggested for cuprates.^{10,11,28} Results do not change qualitatively either with the variation of the parameter t' in Eq. (10) in the range from 0 to $-0.4t$ (notice that parameters t and t' of the hole hopping part of Hamiltonian (3) are only indirectly connected with the coefficients in Eq. (14), since to a great extent the hole dispersion is shaped by the interaction between holes and spin excitations²⁹).

3. Magnetic susceptibility

The momentum dependence of $\chi''(\mathbf{k}\omega)$ calculated with the above equations for three energy transfers are shown in Fig. 2. The contour plots of the susceptibility for the same parameters are demonstrated in Fig. 3. As seen from these figures, there are three frequency regions with different shapes of the momentum dependence of $\chi''(\mathbf{k}\omega)$. The first region is the vicinity of the frequency $\omega_{\mathbf{Q}}$ of the gap in the dispersion of spin excitations at the antiferromagnetic wave vector \mathbf{Q} . For the parameters of Fig. 2 $\omega_{\mathbf{Q}} \approx 37$ meV. In this region the susceptibility is peaked at the wave vector \mathbf{Q} . For smaller and larger frequencies the magnetic response is incommensurate. The dispersion of maxima in $\chi''(\mathbf{k}\omega)$ for scans along the edge and the diagonal of the Brillouin zone and their full widths at half maximum (FWHM) are shown in Fig. 4. Analogous dispersion was obtained in Ref. 28 in the itinerant-carrier approach for the superconducting state.

The momentum dependencies of the susceptibility which are similar to those shown in Fig. 2 and 3 were observed in yttrium and lanthanum cuprates.^{3,4,9} The dispersion of the peaks in $\chi''(\mathbf{k}\omega)$ which is similar to that shown in Fig. 4 was derived from experimental data in $\text{YBa}_2\text{Cu}_3\text{O}_{7-y}$ and $\text{La}_{2-x}\text{Ba}_x\text{CuO}_4$ in Refs. 4, 9. As seen from Fig. 2, for frequencies $\omega < \omega_{\mathbf{Q}}$ the susceptibility is peaked at the wave vectors $\mathbf{k} = (\frac{1}{2}, \frac{1}{2} \pm \delta)$ and $(\frac{1}{2} \pm \delta, \frac{1}{2})$, while for $\omega > \omega_{\mathbf{Q}}$ the maxima are located at $(\frac{1}{2} \pm \delta, \frac{1}{2} \pm \delta)$, $(\frac{1}{2} \pm \delta, \frac{1}{2} \mp \delta)$ for the parameters used. This result is also in agreement with experimental observations.^{4,8,9} Notice, however, that for $\omega > \omega_{\mathbf{Q}}$ the positions of maxima in the momentum space may vary with parameters.

To understand the above results one should notice that Eq. (7) contains the resonance denominator which will dominate in the momentum dependence for $\omega \geq$

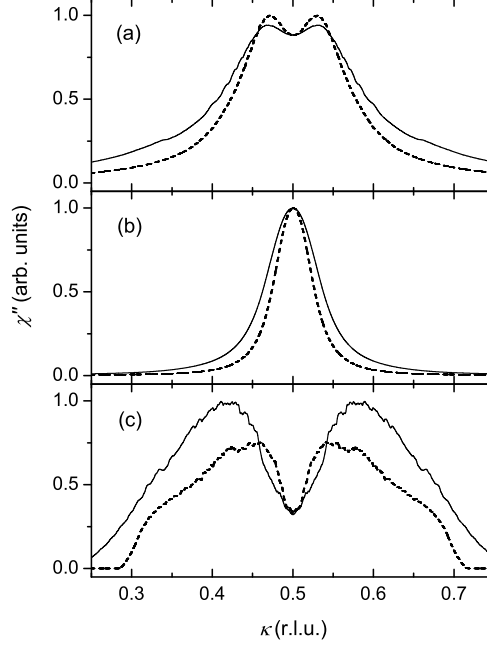


Fig. 2. The momentum dependence of $\chi''(\mathbf{k}\omega)$ for $T = 0$, $x \approx 0.12$, $\mu = -40$ meV, $t' = -0.2t$ and $\omega = 70$ meV, $\eta = 30$ meV (a), $\omega = 35$ meV, $\eta = 15$ meV (b), $\omega = 2$ meV, $\eta = 1.5$ meV (c). Calculations were carried out in a 1200×1200 lattice. The solid lines correspond to the scans along the edge of the Brillouin zone, $\mathbf{k} = (\kappa, \frac{1}{2})$; the dashed lines are for the zone diagonal, $\mathbf{k} = (\kappa, \kappa)$.

$\omega_{\mathbf{Q}}$ if the spin excitations are not overdamped. Parameters of Fig. 2 correspond to this case. For $\omega \geq \omega_{\mathbf{Q}}$ the equation $\omega = \omega_{\mathbf{k}}$ determines the positions of the maxima in $\chi''(\mathbf{k}\omega)$ which are somewhat shifted by the momentum dependence of the spin-excitation damping $f_{\mathbf{k}}\Im R(\mathbf{k}\omega)$. Using Eq. (12) we find that the maxima in $\chi''(\mathbf{k}\omega)$ are positioned near a circle centered at \mathbf{Q} with the radius $c^{-1}(\omega^2 - \omega_{\mathbf{Q}}^2)^{1/2}$.^{16,17}

In the region $\omega < \omega_{\mathbf{Q}}$ the nature of the incommensurability is completely different. It is most easily seen in the limit of small frequencies when Eq. (7) reduces to

$$\chi''(\mathbf{k}\omega) \approx -4\mu_B^2\omega \frac{\Im R(\mathbf{k}\omega)}{\omega_{\mathbf{k}}^4}. \quad (15)$$

As seen in Fig. 1, $\omega_{\mathbf{k}}^{-4}$ is a decreasing function of the difference $\mathbf{k} - \mathbf{Q}$ which acts in favor of a commensurate peak. However, if $\Im R(\mathbf{k}\omega)$ in the numerator of Eq. (15) has a pronounced dip at \mathbf{Q} the commensurate peak splits into several incommensurate maxima. For hole concentrations $x \lesssim 0.06$, when the Fermi surface consists of four ellipses centered at $(\pm\frac{1}{4}, \pm\frac{1}{4})$,^{21,29,30} $\Im R(\mathbf{k}\omega)$ has a dip at \mathbf{Q} due to the nesting of the ellipses with this wave vector.¹⁸ For larger x the mechanism of the dip formation is the following. As follows from Eq. (13), for $\mathbf{k} = \mathbf{Q}$ and small frequencies ω hole states which make the main contribution to the spin-excitation damping (8) are located

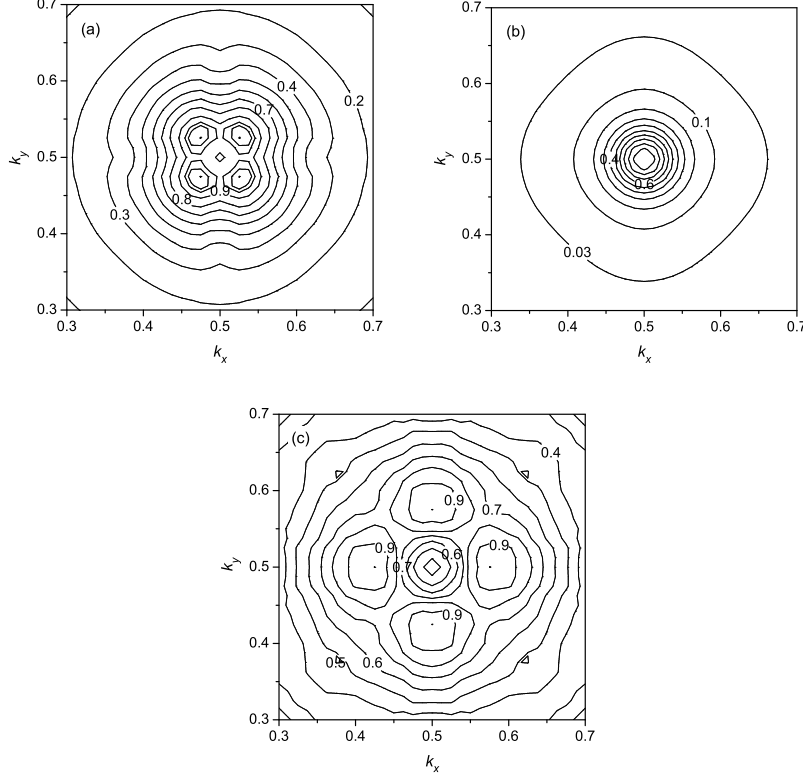


Fig. 3. The contour plots of $\chi''(\mathbf{k}\omega)$. Parameters in parts (a), (b) and (c) are the same as in the respective parts of Fig. 2.

near the hot spots (see Fig. 5). For these wave vectors the interaction constant $g_{\mathbf{Q}\mathbf{k}'}$, Eq. (10), is small which leads to the smallness of $\Im R(\mathbf{Q}\omega)$. With the wave vector moving away from \mathbf{Q} momenta of states contributing to the spin-excitation damping recede from the hot spots, the interaction constant grows, and with it the spin-excitation damping. Thus, the damping has a dip at \mathbf{Q} which leads to the low-frequency incommensurability shown in Fig. 2c.

Let us compare the discussed mechanisms of the low- and high-frequency incommensurability with those based on the picture of itinerant electrons and the random phase approximation. In this latter approach incommensurability arises due to maxima in the noninteracting susceptibility χ_0 described by the fermion bubbles.^{10,11,28} For low frequencies such a maximum appears if the Fermi surface has nesting. As mentioned, this mechanism imposes rather stringent requirements on the electron energy spectrum, because to reproduce known experimental results the nesting has to persist in the wide range of hole concentrations and the nesting momentum has to change in a specific manner with doping. In Ref. 11 the notion was proposed that the nesting for constant-energy contours can appear in the superconducting state.

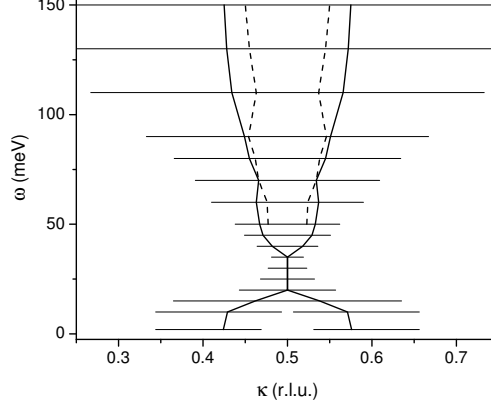


Fig. 4. The dispersion of maxima in $\chi''(\mathbf{k}\omega)$ for scans along the edge [$\mathbf{k} = (\kappa, \frac{1}{2})$, solid lines] and the diagonal [$\mathbf{k} = (\kappa, \kappa)$, dashed lines] of the Brillouin zone. The dispersion along the diagonal is shown only in the frequency range in which these maxima are more intensive than those along the edge. Parameters are the same as in Fig. 2. Horizontal bars are FWHM for maxima along the edge of the Brillouin zone.

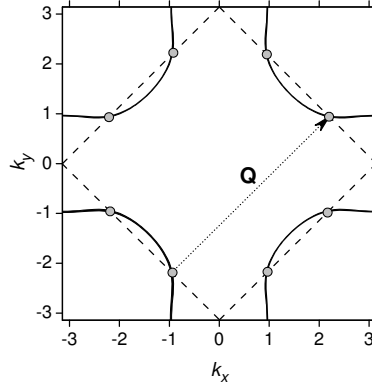


Fig. 5. The Fermi surface for dispersion (14) and $\mu = -40$ meV (solid lines). Dashed lines show the boundary of the magnetic Brillouin zone, gray circles are the hot spots, the dotted arrow is the antiferromagnetic wave vector.

The application of this idea also requires fine tuning of parameters.²⁸ Besides, this mechanism cannot explain the incommensurability above T_c which is observed both in lanthanum and yttrium cuprates.^{3,4,9} In the approach discussed in this paper requirements on the Fermi surface are substantially relaxed: the Fermi surface has to intersect with the boundary of the magnetic Brillouin zone, i.e. the Fermi surface has to contain hot spots where the interaction constant $g_{\mathbf{k}\mathbf{k}'}$ is small which leads to the dip in $\Im R$ at \mathbf{Q} . According to the available photoemission data^{13,30} Fermi surfaces of this type, which resemble that shown in Fig. 5, are indeed observed in underdoped cuprates. Apart from Eq. (14) we used some other model dispersions present in the literature^{10,11,28} and obtained results which are qualitatively similar

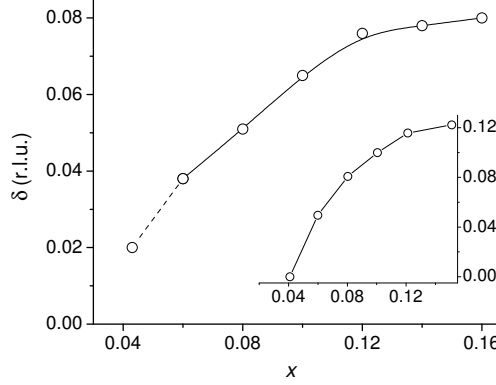


Fig. 6. The incommensurability parameter δ vs. x for $\omega = 2$ meV. The value of δ for $x = 0.043$ was taken from Ref. 18. Inset: experimental data² for $\text{La}_{2-x}\text{Sr}_x\text{CuO}_4$. Connecting lines are a guide to the eye.

to those shown in Fig. 2 – 4. Hence the discussed mechanism is robust with respect to changes of the hole energy spectrum, provided that the Fermi surface contains hot spots. The mechanism is equally applicable for the superconducting state, since the same interaction constant $g_{\mathbf{k}\mathbf{k}'}$ enters into the expression for the susceptibility in this state.¹⁷ We suppose that in certain conditions the magnetic incommensurability may trigger the corrugation of Cu-O planes and formation of stripes.

The dependence of the incommensurability parameter δ on x for the low frequencies is shown in Fig. 6. In agreement with experiment (see the inset in Fig. 6) δ grows nearly linearly with x up to $x \lesssim 0.12$ and then saturates. In this calculation dispersion (14) was used for the entire range of hole concentrations $0.06 \leq x \leq 0.16$. This is not quite correct, since the photoemission data³⁰ and calculations²⁹ demonstrate that the dispersion changes substantially with doping. However, we suppose that the growth of the spin-excitation frequency with doping in accord with the relations $\omega_{\mathbf{Q}} \propto \xi^{-1} \propto x^{1/2}$,²⁵ which leads to a weaker momentum dependence in Eq. (12) and in the denominator of Eq. (15), is more essential for the dependence $\delta(x)$ than the variation of the hole dispersion.

We found also that the low-frequency incommensurability disappears when the hole damping η is greater than ω . Besides, this incommensurability disappears if the chemical potential μ approaches the extended van Hove singularities at $(0, \frac{1}{2})$, $(\frac{1}{2}, 0)$. In this case for $\mathbf{k} = \mathbf{Q}$ the entire region of these singularities in which the interaction constant $g_{\mathbf{Q}\mathbf{k}'}$ is not small contributes to the spin-excitation damping. As a result the dip in the damping becomes shallower or disappears completely. In the t - J model, μ approaches the van Hove singularities for $x \approx 0.18$ for the parameters of hole-doped cuprates.²⁹ This may be the reason of the disappearance of the incommensurability in overdoped cuprates.² The low-frequency incommensurability disappears also in lattices with size less than 30×30 sites. The use of a smaller lattice and an increased artificial broadening needed for stabilizing the it-

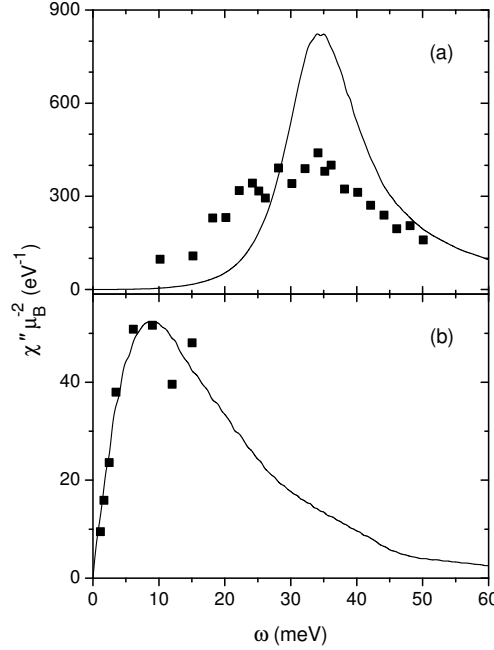


Fig. 7. The frequency dependence of χ'' . The solid lines are our results for $T = 0$, $x \approx 0.12$, $\mu = -40$ meV, $\eta = 3.5$ meV, $\mathbf{k} = \mathbf{Q}$ (a) and for $\mathbf{k} = (0.42, 0.5)$ with the hole dispersion scaled by the factor 0.4 (b, see text). Squares are the odd susceptibility measured⁵ in the normal-state $\text{YBa}_2\text{Cu}_3\text{O}_{6.83}$ ($x \approx 0.14$, 26) at $T = 100$ K and $\mathbf{k} = \mathbf{Q}$ (a) and the susceptibility in $\text{La}_{1.86}\text{Sr}_{0.14}\text{CuO}_4$ for $T = 35$ K at the incommensurate peak⁶ (b).

eration procedure accounts for the lack of low-frequency incommensurability in the self-consistent calculations of Ref. 25.

As mentioned above, for the parameters chosen spin excitations are not overdamped near the antiferromagnetic wave vector. As a consequence, the frequency dependence of $\chi''(\mathbf{Q}\omega)$ has a pronounced maximum at $\omega \approx \omega_{\mathbf{Q}}$ which resembles the susceptibility observed in the underdoped $\text{YBa}_2\text{Cu}_3\text{O}_{7-y}$ in the superconducting and normal states. As seen in Fig. 7a, the experimental width of the maximum is approximately twice as large as the calculated one. Partly this is connected with the difference in temperatures for the two sets of the data. Besides, the width and shape of the frequency dependence of χ'' vary essentially with the change of the hole dispersion and damping. Figure 7b demonstrates that, in particular, the decrease of the hole bandwidth leads to a substantial growth of the spin-excitation damping which in its turn results in the overdamping of spin excitations. For this figure the calculated results were obtained with dispersion (14) scaled by the factor 0.4. The calculations were carried out for $\mathbf{k} = (0.42, 0.5)$ which corresponds to the wave vector of the low-frequency peak in Fig. 2c. The overdamping of spin excitations leads to the red shift of the maximum in $\chi''(\omega)$. Its position is no longer connected with the frequency of spin excitations. The similar frequency dependence of χ'' without

a well-defined peak of spin excitations is observed in $\text{La}_{2-x}\text{Sr}_x\text{CuO}_4$.⁶ Thus, we suppose that the observed dissimilarity of the frequency dependencies of the susceptibility in lanthanum and yttrium cuprates is connected with the different values of the spin-excitation damping.

The increased spin-excitation damping obtained above with the scaled hole dispersion does not affect markedly the low-frequency incommensurability, however, for the frequencies $\omega_{\mathbf{Q}} \geq \omega \geq 150$ meV we found only broad commensurate maxima instead of the incommensurate peaks shown in Fig. 2a. Such spectra are also observed experimentally.¹⁹

Our consideration was restricted to the normal state. In the considered approach the opening of the superconducting gap suppresses the spin-excitation damping for frequencies below the gap and increases the damping above it. The respective redistribution of the intensity takes place also in the susceptibility.^{3,6,16,17} As mentioned, for the momentum dependence the same mechanisms which lead to the incommensurate magnetic response in the normal state operate also in the superconducting state. In this state the suppressed spin-excitation damping produces sharper peaks in the susceptibility, however, their location in the momentum space is approximately the same as in the normal state.^{4,14}

4. Concluding remarks

Mori's projection operator formalism and the t - J model of Cu-O planes were used for the interpretation of the magnetic susceptibility in normal-state cuprate perovskites. It was shown that the calculated momentum and frequency dependencies of the imaginary part of the susceptibility χ'' , the dispersion and location of maxima in it and the concentration dependence of the incommensurability parameter are similar to those observed in lanthanum and yttrium cuprates. The dispersion of the maxima in χ'' resembles two parabolas with upward- and downward-directed branches which converge at the antiferromagnetic wave vector \mathbf{Q} and at the respective frequency of spin excitations $\omega_{\mathbf{Q}}$. This frequency corresponds to a local minimum in the dispersion of spin excitations and its value is connected with the correlation length of the short-range antiferromagnetic order. We relate the upper parabola to the spin-excitation dispersion. The incommensurability connected with the lower parabola is related to the dip in the spin-excitation damping at \mathbf{Q} . For moderate doping the dip arises due to the smallness of the interaction between spin excitations and holes near the hot spots, which is a consequence of the short-range character of this interaction. In agreement with experiment the incommensurate peaks which form the lower parabola are located at momenta $(\frac{1}{2}, \frac{1}{2} \pm \delta)$ and $(\frac{1}{2} \pm \delta, \frac{1}{2})$, while peaks in the upper parabola are at $(\frac{1}{2} \pm \delta, \frac{1}{2} \pm \delta)$ and $(\frac{1}{2} \pm \delta, \frac{1}{2} \mp \delta)$. Also in agreement with experiment the low-frequency incommensurability parameter δ grows linearly with the hole concentration x for $x \lesssim 0.12$ and then saturates. This behavior of δ is mainly connected with the concentration dependence of the frequency $\omega_{\mathbf{Q}}$ of the spin gap at the antiferromagnetic wave vector. We found that the

incommensurability for the transfer frequencies $\omega < \omega_{\mathbf{Q}}$ disappears if the damping of holes with energies $\pm\omega$ is greater than ω . This incommensurability vanishes also when the chemical potential approaches the extended van Hove singularities at $(0, \frac{1}{2})$ and $(\frac{1}{2}, 0)$. The incommensurability for $\omega > \omega_{\mathbf{Q}}$ disappears for large spin-excitation damping. The value of this damping depends heavily on the hole damping and on the shape and width of the hole band. We suppose that the marked difference in the frequency dependencies of the susceptibility in $\text{YBa}_2\text{Cu}_3\text{O}_{7-y}$ and $\text{La}_{2-x}\text{Sr}_x\text{CuO}_4$ – a pronounced peak at $\omega \approx 25 - 40$ meV for $\mathbf{k} = \mathbf{Q}$ in the former crystal and a broad feature at $\omega \approx 10$ meV in the latter – is a consequence of the difference in the electron spectra. The larger spin-excitation damping in $\text{La}_{2-x}\text{Sr}_x\text{CuO}_4$ leads to overdamping of spin excitations, while in the underdoped $\text{YBa}_2\text{Cu}_3\text{O}_{7-y}$ the excitations are well-defined even in the normal state.

Acknowledgements

This work was partially supported by the ESF grant No. 5548 and by the DFG.

References

1. H. Yoshizawa, S. Mitsuda, H. Kitazawa, and K. Katsumata, *J. Phys. Soc. Jpn.* **57**, 3686 (1988); R. J. Birgeneau, Y. Endoh, Y. Hidaka, K. Kakurai, M. A. Kastner, T. Murakami, G. Shirane, T. R. Thurston, and K. Yamada, *Phys. Rev.* **B39**, 2868 (1989).
2. K. Yamada, C. H. Lee, K. Kurahashi, J. Wada, S. Wakimoto, S. Ueki, H. Kimura, Y. Endoh, S. Hosoya, G. Shirane, R. J. Birgeneau, M. Greven, M. A. Kastner, and Y. J. Kim, *Phys. Rev.* **B57**, 6165 (1998).
3. T. E. Mason, G. Aeppli, S. M. Hayden, A. P. Ramirez, and H. A. Mook, *Phys. Rev. Lett.* **71**, 919 (1993); M. Matsuda, K. Yamada, Y. Endoh, T. R. Thurston, G. Shirane, R. J. Birgeneau, M. A. Kastner, I. Tanaka, and H. Kojima, *Phys. Rev.* **B49**, 6958 (1994).
4. P. Dai, H. A. Mook, and F. Dogan, *Phys. Rev. Lett.* **80**, 1738 (1998); M. Arai, T. Nishijima, Y. Endoh, T. Egami, S. Tajima, K. Tamimoto, Y. Shiohara, M. Takahashi, A. Garrett, and S. M. Bennington, *Phys. Rev. Lett.* **83**, 608 (1999); P. Bourges, Y. Sidis, H. F. Fong, L. P. Regnault, J. Bossy, A. Ivanov, and B. Keimer, *Science* **288**, 1234 (2000).
5. P. Bourges, in *The Gap Symmetry and Fluctuations in High Temperature Superconductors*, ed. J. Bok, G. Deutscher, D. Pavuna, and S. A. Wolf (Plenum Press, New York, 1998), p. 349; H. He, Y. Sidis, P. Bourges, G. D. Gu, A. Ivanov, N. Koshizuka, B. Liang, C. T. Lin, L. P. Regnault, E. Schoenherr, and B. Keimer, *Phys. Rev. Lett.* **86**, 1610 (2001).
6. G. Aeppli, T. E. Mason, S. M. Hayden, H. A. Mook, and J. Kulda, *Science* **279**, 1432 (1997).
7. S. M. Haiden, G. Aeppli, H. A. Mook, T. G. Perring, T. E. Mason, S.-W. Cheong, and Z. Fisk, *Phys. Rev. Lett.* **76**, 1344 (1996).
8. S. M. Haiden, H. A. Mook, P. Dai, T. G. Perring, and F. Doğan, *Nature* **429**, 531 (2004).
9. J. M. Tranquada, H. Woo, T. G. Perring, H. Goka, G. D. Gu, G. Xu, M. Fujita, and K. Yamada, *Nature* **429**, 534 (2004).

10. D. Z. Liu, Y. Zha, and K. Levin, *Phys. Rev. Lett.* **75**, 4130 (1995); N. Bulut and D. J. Scalapino, *Phys. Rev.* **B53**, 5149 (1996).
11. J. Brinckmann and P. A. Lee, *Phys. Rev. Lett.* **82**, 2915 (1999).
12. V. Hizhnyakov and E. Sigmund, *Physica* **C156**, 655 (1988); J. Zaanen and O. Gunnarsson, *Phys. Rev.* **B40**, R7391 (1989); K. Machida, *Physica* **C158**, 192 (1989).
13. A. Ino, C. Kim, M. Nakamura, T. Yoshida, T. Mizokawa, A. Fujimori, Z.-X. Shen, T. Kakeshita, H. Eisaki and S. Uchida, *Phys. Rev.* **B65**, 094504 (2002).
14. H. Kimura, K. Hirota, H. Matsushita, K. Yamada, Y. Endoh, S.-H. Lee, C. F. Majkrzak, R. Erwin, G. Shirane, M. Greven, Y. S. Lee, M. A. Kastner, and R. J. Birgeneau, *Phys. Rev.* **B59**, 6517 (1999); M. Fujita, H. Goka, K. Yamada, and M. Matsuda, *Phys. Rev. Lett.* **88**, 167008 (2002).
15. H. Mori, *Progr. Theor. Phys.* **34**, 399 (1965); S. Onoda and M. Imada, *J. Phys. Chem. Solids* **63**, 2225 (2002).
16. V. Barzykin and D. Pines, *Phys. Rev.* **B52**, 13585 (1995).
17. A. Sherman and M. Schreiber, *Phys. Rev.* **B65**, 134520 (2002); **68**, 094519 (2003).
18. A. Sherman and M. Schreiber, *Phys. Rev.* **B69**, 100505(R) (2004).
19. Y. Endoh, T. Fukuda, S. Wakimoto, M. Arai, K. Yamada, and S. M. Bennington, *J. Phys. Soc. Japan* **69**, Suppl. B, 16 (2000).
20. M. A. Kastner, R. J. Birgeneau, G. Shirane, and Y. Endoh, *Rev. Mod. Phys.* **70**, 897 (1998).
21. Yu. A. Izyumov, *Usp. Fiz. Nauk* **167**, 465 (1997) [*Phys.-Usp. (Russia)* **40**, 445 (1997)]; E. Dagotto, *Rev. Mod. Phys.* **66**, 763 (1994).
22. F. C. Zhang and T. M. Rice, *Phys. Rev.* **B37**, 3759 (1988).
23. J. H. Jefferson, H. Eskes and L. F. Feiner, *Phys. Rev.* **B45**, 7959 (1992); A. V. Sherman, *Phys. Rev.* **B47**, 11521 (1993).
24. J. Kondo and K. Jamaai, *Progr. Theor. Phys.* **47**, 807 (1972); H. Shimahara and S. Takada, *J. Phys. Soc. Japan* **60**, 2394 (1991); S. Winterfeldt and D. Ihle, *Phys. Rev.* **B56**, 5535 (1997).
25. A. Sherman and M. Schreiber, *Eur. Phys. J.* **B32**, 203 (2003).
26. J. L. Tallon, C. Bernhard, H. Shaked, R. L. Hitterman, and J. D. Jorgensen, *Phys. Rev.* **B51**, R12911 (1995).
27. A. K. McMahan, J. F. Annett, and R. M. Martin, *Phys. Rev.* **B42**, 6268 (1990); V. A. Gavrichkov, S. G. Ovchinnikov, A. A. Borisov, and E. G. Goryachev, *Zh. Eksp. Teor. Fiz.* **118**, 422 (2000) [*JETP (Russia)* **91**, 369 (2000)].
28. M. R. Norman, *Phys. Rev.* **B61**, 14751 (2000).
29. A. Sherman, *Phys. Rev.* **B70**, 184512 (2004).
30. A. Damascelli, Z. Hussain, and Z.-X. Shen, *Rev. Mod. Phys.* **75**, 473 (2003).